Effect of Annealed (0001) α-Al_2O_3 Surfaces on Heteroepitaxial Growth of Silver Nanoparticles

A. Al-Mohammad*
Nano-materials Labs, Physics Department, Atomic Energy Commission of Syria
P.O. Box 6091, Damascus, Syria

(Received March 27, 2008; revised version September 18, 2008)

The effect of annealed (0001) α-Al_2O_3 surfaces on heteroepitaxial growth of silver nanoparticles were analysed by reflection high-energy electron diffraction, transmission electron microscope and selected area electron diffraction. Ag nanoparticles were deposited on 1×1 stoichiometric and reconstructed (111)Al//(0001) α-Al_2O_3 with the Knudsen cell. The maximum cluster density method and the Lifethenz theory of Van der Waals energy were used to investigate the Ag//(0001)α-Al_2O_3 interface parameters. The growth modes, lattice parameters, nanoparticle forms and sizes are strongly dependent on the substrate surface structures. Initially, three-dimensional islands of Ag nanoparticles grow on both kinds of surfaces with partial hexagonal shapes. Ag nanoparticles on stoichiometric surface create the (111)Ag//(0001)α-Al_2O_3 interface without any preferred epitaxial direction. On this surface, Gaussian distribution is characteristic of an atom-by-atom growth mode with density of Ag nanoparticles lower than saturation density while a coalescence growth mode appears due to binary collisions between Ag nanoparticles accompanied by a liquid-like behaviour after saturation density. In case of reconstruction substrates, the epitaxial relationships between Ag nanoparticles and the surface are formed (111)Ag//(0001)α-Al_2O_3, $\langle 01\bar{1}\rangle$Ag//$[12\bar{3}0]\alpha$-Al_2O_3 or $\langle 01\bar{1}\rangle$Ag//$[1\bar{1}00]\alpha$-Al_2O_3. The Ag nanoparticles make rotation with angles between $\pm 6^\circ$ around the epitaxial orientations $\langle 1\bar{1}00\rangle$ or $\langle 12\bar{3}0\rangle$. Only the atom-by-atom growth mode were found at all Ag nanoparticles growth processes.

PACS numbers: 68.55.−a, 81.15.Aa, 61.05.jh, 61.46.Df

1. Introduction

Advances in nanomaterial technologies allow the synthesis of well defined nanoscaled solid objects. These so-called nanoparticles (NPs) or clusters, they are fabricated with high reproducibility. Metal-oxide and other ceramic surfaces covered by metal NP films play an important role in many fields of nanomaterials technologies, including metal–matrix composites in various nanoelectronic uses, quantum dots, heterogeneous catalysis, etc. [1, 2]. In all cases, the interfacial region between metal and oxide at the atomic scale is vital to ensure a continued and controlled improvement of these materials and of their use in different technological devices [1–3]. The most technologically widespread metal–ceramic systems are noble metals//α-Al_2O_3 especially silver NPs//(0001)α-Al_2O_3 system for its many applications as an antimicrobial, antibacterial, antibiotic, antifungal agents, fibres, polymers, first aid bandages, plastics, textiles, nanodevices and gas sensors [1–7]. Growth mode, crystalline structure, morphology, grain size and other properties of silver powder or thin films on α-Al_2O_3 surfaces started to be studied in the 1980s. Various techniques make possible the determination of the crystallographic and electronic structure of (0001) α-Al_2O_3 surfaces and giving evidence that the surface structure is modified by thermal treatments [5]. It has been shown in Refs. [8–11] that the thermal treatments under vacuum are responsible for the (0001) α-Al_2O_3 surface reducibility. Generally, an increase in annealed temperature of α-Al_2O_3 surfaces results in formation of a thin aluminium-rich layer giving the excitation of aluminium surface plasmons. An important change in silver NPs properties as particles sizes, shapes, growth modes occur in the structural deformations of α-Al_2O_3 surfaces.

The purpose of this work is to understand the effect of the structure modifications of the (0001) α-Al_2O_3 surfaces on growth parameters of Ag NPs. The reflection high-energy electron diffraction (RHEED), transmission electron microscopy (TEM) and compatible selected area electron diffraction (SAED) were used in study of growth modes, adsorption energies, lattice parameters and heteroepitaxial relationships of Ag NPs//(0001) α-Al_2O_3 systems.

2. Experimental

The α-Al_2O_3 samples are thin slides cut in single alumina crystal grown by the Czochralski method and chem-

* e-mail: scientific@aec.org.sy, aamohammad@aec.org.sy

ically polished. Specimens are cut so that the (0001) crystallographic plane is parallel to the surface. After cleaning in alcohol, the (0001) α-Al_2O_3 surfaces were annealed under vacuum better than 10^{-3} Pa for 3 h at 1100 K (A substrates) or 2000 K (B substrates). We have tested the surface composition, the morphology and the crystallographic structure using the Auger electron spectroscopy (AES), atomic force microscopy (AFM) and RHEED methods.

The silver NPs are carried out from the Knudsen cell simultaneously on the A and B substrates in a high vacuum chamber (Elettrorava, Italy). The A and B substrates have the same size (5 mm × 5 mm × 0.3 mm) and are placed near one to another on the same heating support at a distance of 15 cm from the vapour source. In each experiment, the two substrates received the same quantity of silver. They were at the same deposition temperature $T_d = 550$ K and the same pressure $P \approx 10^{-4}$ Pa. The deposition rate and the mean deposit thickness were monitored by a quartz balance at a rate of 0.3–0.4 ML/min (1 ML = 1.407×10^{15} atoms/cm^2: (111) Ag). For the purpose of determining the maximum particles density N_s of Ag NPs the mean deposit thickness was varied from 0.5 to 5 nm with a step of 0.5 nm. The morphology and crystalline structure of substrate surfaces and silver NPs were investigated by means of RHEED (Elettrorava, Italy), TEM and SAED (Siemens102, acceleration voltage 125 KV). The RHEED system configuration enables us to observe the diffraction pattern during the epitaxial growth of Ag NPs. The A and B substrates are fixed on a movable sample holder permitting to heat them, to measure their temperatures and to change the angle of incidence beam as well as the azimuthal direction of electron beams. All the RHEED patterns of substrates before and after Ag NPs deposition were effected *in situ* (the annealing of substrates and the Ag NPs deposition in the same vacuum system). The Ag NPs were detached from substrates at each step using a carbon replica and HF acid method and examined by TEM. The results of TEM and RHEED methods are identical before and after detaching the replica using HF acid. The RHEED and SAED patterns were digitised using computer systems with a CCD camera in order to obtain the crystallographic structure during the growth processes.

3. Results

3.1. Structure of (0001) α-Al_2O_3 surface

Before the deposition processes the substrates were tested by AFM and RHEED methods. While the non-annealed surfaces exhibit an important roughness (mean value 25 nm), the surfaces annealed at 1100 K are composed of large grains (200 nm) limited by etched grain boundaries with a reduced roughness (mean value 10 nm). We observed RHEED patterns with the Kicuchi lines and Laue zones characteristic of a (1 × 1) α-Al_2O_3 bulk stoichiometric structure. The (0001) α-Al_2O_3 surfaces annealed at 2000 K exhibit large facets separated by multiatomic steps. On these surfaces, the RHEED observations give rather good diffraction patterns characteristic of a flat surface and provided by large (111) aluminum facets. Details are given in Refs. [5, 8–11]. The reconstructed surface has been already observed by LEED and interpreted as a result of non-stoichiometry of α-Al_2O_3 surface layers and ordering of oxygen vacancies [12].

3.2. Silver nanoparticles granulometry

The results on Ag NP granulometry were obtained in experiments on both A and B surfaces. The particle densities evaluated from the electron micrographs, considering that the densities are measured on substrate surface areas free of steps or defects, which can be revealed by no homogeneities in the particle repartitions. For Ag NPs on both A and B substrates, it was noted that the saturation thickness was 2 nm. At this thickness the substrate surface had a maximum particles density N_s. At the thickness smaller than 2 nm some nucleation sites on substrates were empty. At the thickness larger than 2 nm some particles were coalesced. This operation resulted in some empty sites on substrates. Figures 1 and 2 represent micrographs, SAED patterns, size distributions and histograms of the Ag NPs obtained respectively from the A and B substrates at the saturation thicknesses (2 nm). It appears that the Ag NPs density is larger on A substrate than that on B one. It is evident that the growth kinetics depend on the surface structure induced by different annealing. However, the shapes of size histograms are characteristic of the growth mechanism [13–15]. The histogram corresponding to the Ag NPs on A substrate is composed of two peaks: a small peak fitted by a Gaussian curve and a large one fitted by a log-normal curve. The fitting of histogram which is characteristic of the Ag NP size on the B substrate exhibits only one peak corresponding to a Gaussian distribution. The main granulometric characterisations of deposits on the two kinds of substrate A and B are summarised in Table I.

3.3. Ag NPs//(0001)α-Al_2O_3 heteroepitaxial relationships

The SAED patterns corresponding to the Ag NPs on A substrate exhibit strong $\bar{2}20$ ring which is consistent with Ag NPs having their (111) plane parallel to the substrate without any azimuthal orientation, Fig. 1a. In case of B substrate, Fig. 2a, epitaxial patterns exhibit the $\bar{2}20$ diffraction spots with ring arc shaped corresponding to a central angle of about 12°. Generally, the RHEED patterns corresponded to the Ag NPs on A substrate exhibit rings with good contrast characteristic of small crystallites and most of them have a (111) plane parallel to the substrate surfaces. The RHEED patterns of the Ag NPs on the B substrate exhibit spots like diffraction by transmission, which indicated formation of three-dimensional NP growth. Figure 3 shows the RHEED patterns and corresponding simulated diagrams of Ag NPs grown on A

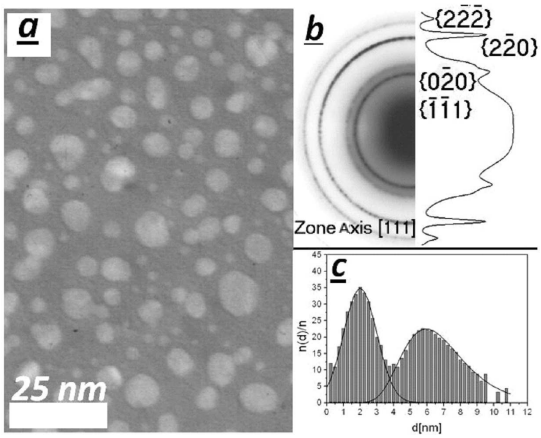

Fig. 1. (a) TEM micrograph; (b) its SAED pattern with (111) Ag NPs are parallel to substrate surfaces; (c) size distribution and histogram of Ag NPs deposited on stoichiometric (0001) α-Al_2O_3 surfaces (A substrates).

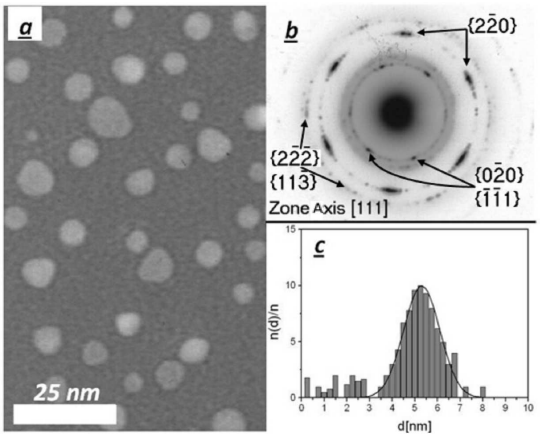

Fig. 2. (a) TEM micrograph; (b) its SAED pattern (111) with Ag NPs have following heteroepitaxial relationship: (111)Ag//(0001)α-Al_2O_3 and ⟨01$\bar{1}$⟩Ag//[12$\bar{3}$0]α-Al_2O_3, (c) size distribution and histogram of Ag NPs deposited on reconstructed (0001) α-Al_2O_3 surfaces (B substrates).

and B substrates at the saturation thicknesses. The incident electron beams are paralleled to the [1$\bar{1}$00] α-Al_2O_3 crystallographic direction. Heteroepitaxial relationships with high reproducibility for all Ag thicknesses on B substrates were found. The interpretation of the RHEED patterns of Ag NPs//B substrates gives the following relationships:

(111) Ag // (0001) α-Al_2O_3,

[$\bar{1}$10] Ag // [$\bar{1}$100]α-A1_2O_3.

A similar mode of growth on alumina has been observed previously for Rh and Au [16] and for Pd on mica [17, 18].

The values of planes spacing $d^c_{(hkl)}$ (where c is Ag, Al, or α-Al_2O_3 compounds, hkl are the crystallographic

TABLE I

Main granulometric characterisations of Ag NPs deposited on (0001) α-Al_2O_3 surfaces (A and B substrates).

Substrate	$N_s \times 10^{12}$ [cm^{-2}]	Gaussian peak at [nm]	Log-normal peak at [nm]	Mean size [nm]	Coverage [%]
A (1100 K)	1.96(6)	2.1(2)	5.8(6)	4.4(7)	28(4)
B (2000 K)	0.59(2)	5.4(6)	–	5.4(6)	19(3)

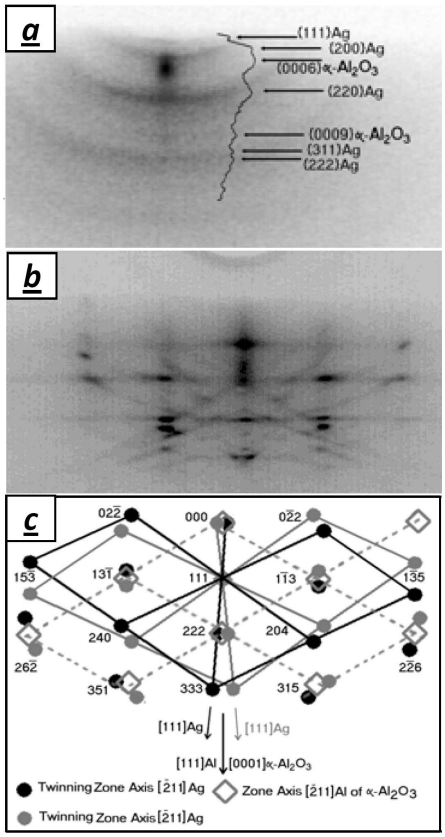

Fig. 3. (a) RHEED pattern and its profile of Ag NPs grown on A substrate with (111)Ag//(0001)α-Al_2O_3; (b) RHEED pattern of Ag NPs grown on B substrates at the saturation thicknesses; (c) corresponding simulated diagrams with following twinned relationships: (111)Ag//(0001)α-Al_2O_3 and [$\bar{1}$10] Ag//[$\bar{1}$100]α-A1_2O_3.

plane indices) in the ⟨$\bar{1}$10⟩ or ⟨111⟩ directions during the growth processes were measured using the intensity profile distance between diffraction spots of the RHEED and SAED patterns. The planes spacing was determined relative to the substrate lattice by measuring the distances between spots in parallel and perpendicular directions to the substrate surfaces. The evolution of the $d^c_{(hkl)}$ parameters as a function of deposition thicknesses is presented in Fig. 4. The values of planes spacing $d^c_{(hkl)}$ of bulk (111) silver and (0001) α-A1_2O_3 oxide were also plotted in. In

case of Ag NPs on A substrate, the values of parallel planes spacing of Ag increased slightly from the $d^{\alpha-\mathrm{Al_2O_3}}_{[1\bar{1}00]}$ to the $d^{\mathrm{Ag}}_{[\bar{1}10]}$ giving a lattice compression. The perpendicular values, $d^{\mathrm{Ag}}_{[111]}$, decreased from 0.236 nm down to the bulk values indicating lattice dilatation. The values of planes spacing of Ag NPs on B substrate remained nearly constant giving short lattice deformations.

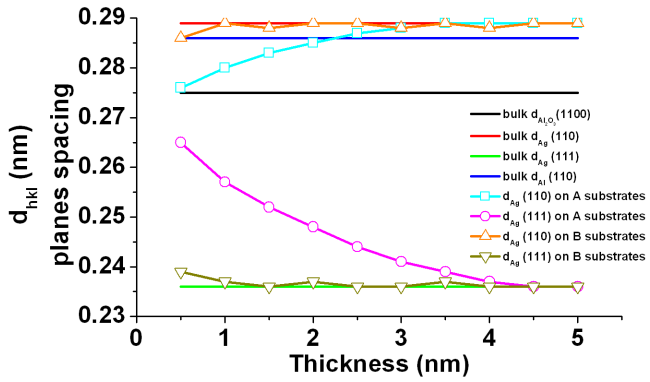

Fig. 4. Evolution of the planes spacing $d^c_{(hkl)}$ as a function of deposition thickness of Ag NPs films. For comparison, the values of $d^c_{(hkl)}$ of bulk {111}, {110} Ag, {110} Al and {1100} α-A1$_2$O$_3$ planes were also plotted.

4. Discussions

Granqvist et al. [19–22] have shown that the particle size distribution following a log-normal function results from a coalescence growth mode due to binary collisions between particles accompanied by a liquid-like behaviour while the Gaussian distribution is characteristic of an atom-by-atom growth mode. Experiments of growth of small metal NPs on oxide substrates have shown that the particle size distribution is influenced by post-nucleation phenomena, in particular by the coalescence. The coalescence is either dynamical resulting from the mobility of small NPs on the substrate surface or static resulting from contact between large neighbouring NPs after lateral growth. Several papers [18, 23–28] have been reported that the dynamical coalescence was first studied by Mac Laughan and proved experimentally by Masson, and the mobility coalescence was introduced into the nucleation theory by Zinsmeister, Venables and Kashchiev. The mobility coalescence was introduced into the nucleation theory by Zinsmeister, Venables and Kashchiev [18, 23–28]. They have shown that the static coalescence is described by deformations in NP forms and only one peak in the size histogram which is fitted by a log-normal curve, while mobility coalescence is described by two peaks which are fitted by Gaussian curve with small size and log-normal curve with deformations in NP forms. Experiments of nucleation and growth of metal deposit on alkali halides have similarly shown that this phenomenon depends on the substrate temperature [29] and on the NP size, so that small NPs can coalesce at room temperature [30–35]. The experimental histograms show that the size distributions of Ag NPs are influenced by the mobility coalescence, which causes the presence of two peaks in the size histogram corresponding to a deposit on A substrate where the NPs density is large. Due to the mobility coalescence some NPs disappear and the corresponding nucleation sites become free for renucleation. Therefore, we make the hypothesis that the total number of Ag NPs is constant and corresponds to the observed maximum density N_s of Ag NPs on the substrate.

TABLE II

Adsorption energy E_a of Ag NPs on stoichiometric and reconstructed (0001) α-Al_2O_3 surfaces (A and B substrates) evaluated from the maximum cluster density method and from the VdW energy of metal–oxide interface with the Lifethenz continuum approximation.

Substrate	$E_\mathrm{a}^\mathrm{MCD}$	W_VDW [J m^{-2}]		$E_\mathrm{a}^\mathrm{VDW}$
	[eV/atom]	W^-_VDW	W^+_VDW	[eV/atom]
A (1100 K)	0.39(8)	0.56(3)	0.85(6)	0.27(4)→0.41(5)
B (2000 K)	0.21(8)	0.37(3)	0.46(6)	0.18(4)→0.22(5)

The crystalline relationships between silver NPs and α-Al_2O_3 surfaces depend on two effects: the first is the mismatch (f) at the Ag//(0001) α-Al_2O_3 interface, the second is the adsorption energy E_a of at the interface [3, 33–35]. We evaluated E_a from the maximum cluster density method (Eq. (1)) and from the Van der Waals (VdW) energy of metal–oxide interface with the Lifethenz continuum approximation (Eq. (2)). Table II resumes the results of E_a in the case of Ag NPs on stoichiometric and reconstructed (0001) α-Al_2O_3 surfaces [3];

$$\left(\frac{N_\mathrm{s}}{N_0}\right)^q (1+\sigma D\tau_\mathrm{a}N_\mathrm{s})^i (Z_0+\sigma D\tau_\mathrm{a}N_\mathrm{s}) = \left(\frac{R}{N_0^2 D}\right)^i \exp(\beta E_i)(D\tau_\alpha N_\mathrm{a})^{i+1}, \quad (1)$$

where $q=\frac{3}{2}$ for 3D nucleation and assuming $i=1$; $C=\sigma D\tau_\mathrm{a}N_\mathrm{s}$; N_0 is the nucleation site density $\approx 1.3\times10^{15}$/cm^2; R is the deposition rate $\approx 8.7\times10^{13}$ at/(cm^2 s); σ is the capture coefficient ≈ 7; τ_a is the atom rest time $=\frac{1}{\nu_\mathrm{a}}\mathrm{e}^{+\beta E_\mathrm{a}^\mathrm{MCD}}$; with $\beta=1/kT$; and $\nu_\mathrm{a}=$ vibration frequency $\approx 1\times10^{13}$; D is the diffusion coefficient $=\alpha\nu\exp(-\beta E_\mathrm{d})/N_0$ with $\alpha=0.25$; the diffusion energy E_d is a fraction of $E_\mathrm{a}^\mathrm{MCD}$; $E_\mathrm{d}=E_\mathrm{a}^\mathrm{MCD}/5$; E_i is the binding energy of a stable nucleus estimated from sublimation energy of metal crystal ($E_i^\mathrm{M}=0.5$ eV/atom):

$$W=\frac{C}{r^6}, \quad (2)$$

where $C=\frac{3}{2}\frac{\alpha_1\alpha_2 I_1 I_2}{I_1+I_2}$ for London dispersion interactions (α_j and I$_j$ are the electronic polarisability and ionisation potential of the j-th species, respectively, when $j=1,2$).

We consider that the misfits are adaping an elastic strain in the first stages of the silver growth [3]. When E_a is large, the energy of VdW between silver atoms and the

substrate is large, the atoms which make the first layer of an Ag NP will take a crystallographic form, which is very similar to atom distributions of the surface substrate. Therefore, if the forms of substrate surfaces and the surface joining of deposit are more different the crystal parameters of interface are more different than the massive ones. From these discussions we can see the role of E_a that can explain the changes of the silver lattice parameter in the first nucleation stage. First silver atoms make the strongest VdW bounds with substrate atoms. Since the interfaces have elastic misfits and the silver atoms will nearly have the same positions of the substrate sites (Ag NPs on stoichiometric (0001)α-Al_2O_3surface). For the second or higher Ag atomic layer, the VdW energy and the misfit values decrease. The Ag lattice parameter increases until bulk state is reached. These changes are in agreement with the experimental, Fig. 4 and Table I. In case of Ag NPs on reconstructed (0001)α-Al_2O_3 surfaces there is a perfect agreement between the adsorption sites on the substrate and the (111) silver plane, the value of the VdW energy is smaller, thus the nucleation and growth processes develop without deformations in the silver parameter.

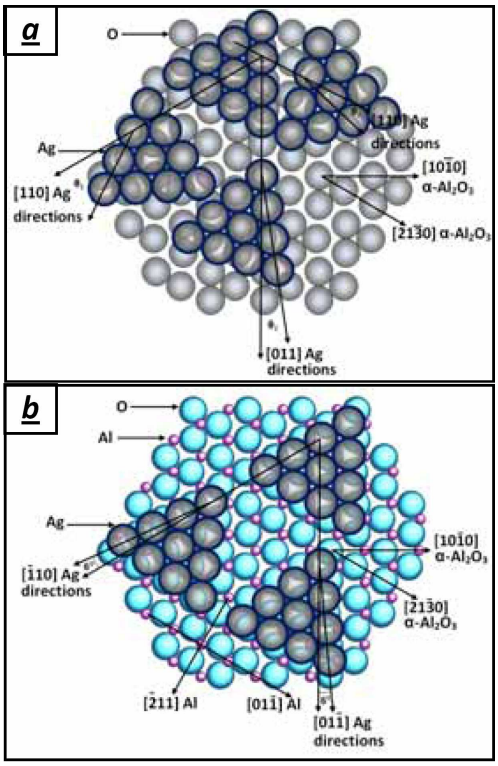

Fig. 5. (a) Model of the deposited Ag NPs on stoichiometric (0001) surfaces. (111)Ag//(0001)α-Al_2O_3 with $\theta_1 \neq \theta_2 \neq \theta_3$; (b) model of the heteroepitaxial relationships between Ag NPs and the reconstructed (0001) surfaces: (111)Ag//(0001)α-Al_2O_3 and $\langle 01\bar{1}\rangle$Ag//[12$\bar{3}$0]α-Al_2O_3 or $\langle 01\bar{1}\rangle$Ag//[1$\bar{1}$00]α-Al_2O_3. Bulk lattice parameters of Ag, Al and α-Al_2O_3 were used for the model constructions.

The RHEED and SAED data made it possible to draw the model of heteroepitaxial relationships between silver NPs and the reconstructed (0001) α-Al_2O_3 surfaces, these models are presented in Fig. 5. It represents the basal plane of the silver over layer onto the (0001) α-Al_2O_3 stoichiometric and reconstructed surfaces. The bulk lattice parameters of substrates and Ag NPs were used for the model constructions. The models show the probable orientations and crystallographic symmetry of the silver NPs relative to the structure of substrate surfaces. Finally, this work confirms an important result which is: the growth of Ag NPs on the stoichiometric (0001) α-Al_2O_3 surfaces likes the 3D islands growth of metal–insulator system, while this growth on the (0001) α-Al_2O_3 reconstructed surfaces is similar to the heteroepitaxial growth of metal–conductor.

5. Conclusion

After vacuum annealing of the (0001) α-Al_2O_3 surfaces, stoichiometric structures 1×1 and reconstruction ones (111)Al//(0001)α-Al_2O_3 appeared for the annealing of 1100 K and 2000 K, respectively. The growth of Ag NPs is carried out for several thicknesses. The heteroepitaxial relations observed between NPs and substrates suggest that the misfit and the interface energy between particles and the substrate surfaces determine the interface formation. These reasons lead to that the growth of silver NPs on the 1×1 of (0001) α-Al_2O_3 surfaces will give more interface dislocations than on reconstructed surfaces. The VdW theory of interface energy matches well the Ag NPs//α-Al_2O_3 couple to explain the heteroepitaxial growth at interface. The Ag NPs grow on the stoichiometric (0001) α-Al_2O_3 surfaces with 3D islands growth mode but they grow on the (0001) α-Al_2O_3 reconstructed surfaces with the heteroepitaxial relationships:

(111) Ag // (0001) α-Al_2O_3
and
$\langle 01\bar{1}\rangle$ Ag // [12$\bar{3}$0]α-Al_2O_3
or
$\langle 01\bar{1}\rangle$ Ag // [1$\bar{1}$00]α-Al_2O_3.

Acknowledgments

I would like to thank Prof. I. Othman, Director General of the Atomic Energy Commission of Syria for his support and encouragement.

References

[1] J.S. Moya, S. Lopez-Esteban, C. Pecharroman, *Prog. Mater. Sci.* **52**, 1017 (2007).

[2] W. Lojkowski, H.J. Fecht, *Prog. Mater. Sci.* **45**, 339 (2000).

[3] L.M. Gruia, F.D. Rochon, A.L. Beauchamp, *Inorg. Chim. Acta* **360**, 1825 (2007).

[4] R. Bredesen, K. Jordal, O. Bolland, *Chem. Eng. Proc.* **43**, 1129 (2004).

[5] M. Gillet, A. Al-Mohammad, *Thin Solid Films* **374**, 134 (2000).

[6] R. Mishra, *Sensors Mater.* **17**, 433 (2005).

[7] T. Yang, G.H. Yu, B.H. Li, T. Suzuki, F.W. Zhu, *Advanced Nanomaterials and Nanodevices*, IUMRS-ICEM, Xian 2002.

[8] C. Lemire, S. Bertarione, A. Zecchina, D. Scarano, A. Chaka, S. Shaikhutdinov, H.-J. Freund, *Surf. Sci.* **572**, 103 (2004).

[9] T. Epicier, C. Esnouf, *J. Phys. III (France)* **4**, 1811 (1994).

[10] M. Gillet, *Surf. Rev. Lett.* **5**, 325 (1998).

[11] S.M. Mukhopadhyay, A.P. Jardine, J.M. Blakely, S.Baik, *J. Am. Ceram. Soc.* **71**, 358 (1998).

[12] Yu.V. Naidich, *Prog. Surf. Membrane Sci.* **14**, 353 (1981).

[13] Don M. Lipkin, *Philos. Mag. A* **76**, 715 (1997).

[14] D. Walton, *J. Chem. Phys.* **37**, 2182 (1962).

[15] M.J. Stowell, *Philos. Mag.* **26**, 361 (1972).

[16] J.E. McDonald, J.G. Eberhart, *Trans. Met. Soc. Aime* **233**, 512 (1965).

[17] H. Poppa, *Ultra Microsc.* **11**, 105 (1983).

[18] M. Gillet, *J. Microsc. Spectrosc. Electron.* **11**, 449 (1986).

[19] E. Gillet, *Z. Phys. D* **19**, 361 (1991).

[20] C.G. Granqvist, R.A. Buhrman, *Appl. Phys. Lett.* **27**, 693 (1975).

[21] C.G. Granqvist, R.A. Buhrman, *Appl. Phys.* **47**, 2200 (1976).

[22] C.G. Granqvist, R.A. Buhrman, *Solid State Commun.* **18**, 123 (1976).

[23] J.A. Venables, G.L. Price, Epitaxial Growth, Academic, New York 1975.

[24] T.M. French, G.A. Somorjai, *J. Phys. Chem.* **74**, 2489 (1970).

[25] S. Baik, C.L. White, *J. Am. Ceram. Soc.* **70**, 682 (1987).

[26] E. Gillet, in: *Science of Ceramic. Interfaces*, Ed. J. Novotny, Elsevier Sci., Amsterdam 1991, p. 439.

[28] T.M. French, G.A. Somorjai, *J. Phys. Chem.* **74**, 2489 (1970).

[29] M. Gautier, J.P. Durand, L. Van Pham, M.J. Guittet, *Surf. Sci.* **250**, 71 (1991).

[30] G. Renaud, B. Vilette, I. Vilfan, A. Bourret, *Phys. Rev. Lett.* **73**, 1825 (1994).

[31] C.C. Chang, *J. Vac. Technol.* **8**, 500 (1971).

[32] E. Gillet, B. Ealet, *Surf. Sci.* **273**, 427 (1992).

[33] N. Eustathopoulos, *J. Phys. III (France)* **4**, 1865 (1994).

[34] C. Noguera, *J. Phys. III (France)* **4**, 1851 (1994).

[35] E. Gillet, *J. Chim. Phys.* **84**, 167 (1987).